Journal of the Mechanics and Physics of Solids
Volume 145, December 2020, 104145

# Mode I fracture toughness determination in Cu/W nano-multilayers by SEM - Digital Image Correlation

[a,*]León Romano Brandt, [a,b]Enrico Salvati, [c]Eric Le Bourhis and [a]Alexander M. Korsunsky

[a]Multi-Beam Laboratory for Engineering Microscopy, Department of Engineering Science, University of Oxford, Parks Road, Oxford OX1 3PJ
[b]Polytechnic Department of Engineering and Architecture (DPIA), University of Udine, Via delle Scienze 208, Udine, 33100, Italy
[c]Institut P', UPR 3346, CNRS - Université de Poitiers, 11 Bd M&P Curie, 86073 Poitiers, France
[*]Corresponding author. Email address : leon.romanobrandt@eng.ox.ac.uk

DOI: https://doi.org/10.1016/j.jmps.2020.104145

Received 9 August 2020, Accepted 1 September 2020, Available online 3 September 2020

## Abstract

Nanostructured metallic multilayers with carefully designed mechanical and functional properties are omnipresent in cutting edge technological applications. To ensure the mechanical integrity of such coatings, the Mode I critical stress intensity factor $K_{IC}$ is used to quantify their fracture toughness in order to avoid material failure by appropriate design. In this article, we present a novel approach for the $K_{IC}$ determination of thin and ultrathin films on compliant substrate, based on micro-displacement field analysis using Digital Image Correlation within SEM. Using this method, $K_{IC}$ of a Cu/W nano-multilayer with a total coating thickness of 240 nm was determined as $K_{IC} = 4.8 \pm 0.05\ \mathrm{MPa}\sqrt{\mathrm{m}}$, showing excellent agreement with the values published for comparable systems in the literature. To verify the validity of the chosen approach, two independent finite element simulations were employed,

thus revealing the role and effect of the compliant substrate on the stress and displacement fields arising around the crack tip in thin films.

## Keywords

Fracture Toughness, Cu/W nano-multilayer, Thin Film, Digital Image Correlation, Finite Element Simulation

## Highlights

- Fracture toughness of Cu/W nano-multilayers on Kapton substrate was determined using Digital Image Correlation
- Finite Element Simulation confirmed validity of chosen approach
- Local plastic deformation of substrate was identified as driver underlying crack opening
- Obtained fracture toughness showed excellent agreement with literature values

## 1. Introduction

Crack nucleation and propagation in thin films and coatings may cause premature failure under external load. A multitude of interdependent factors influence the fracture resistance in such materials, such as the intrinsic microstructural properties, the balance between ductile and brittle responses, and the residual stress state resulting from the manufacturing history [1], as well as the type and direction of applied loading. A theory frequently employed in engineering design for brittle and semi-brittle materials is Linear Elastic Fracture Mechanics (LEFM). This popular failure criterion relies on the determination of the Stress Intensity Factor (SIF) that describes the elastic deformation fields in an annular region surrounding the crack tip, also known as K-field. Failure is expected to occur once the critical value of the SIF is reached, for instance, $K_{IC}$ for pure mode I loading. $K_{IC}$ can be readily determined for bulk materials using standardised mechanical testing procedures. When evaluating the fracture properties of thin and ultra-thin materials, however, standard test procedures cannot be applied. A multitude of adapted approaches [2] have therefore been developed and presented in the past: bending [3,4], buckling [5,6], scratching [7,8], micro-cantilever indentation [9,10], bulge testing [11], as well as nano-indentation [12,13] tests have proven successful at determining the critical parameters for failure criteria. Unfortunately, extensive sample preparation [3,11] is often times required, which involves the risk of modifying the coating structure and its response to loading. Focused

Ion Beam (FIB) preparation of nano-scale cantilevers, for instance, can significantly modify the mechanical properties within surface layers affected by ion implantation [14,15]. Furthermore, these test methods are often limited to film thicknesses of several microns, which makes testing of sub-micron to sub-nanometre thin films hardly feasible.

Nowadays, cutting-edge developments in electronics and surface modification rely on ultra-thin films and coatings that exhibit carefully designed material properties at the (sub-) nanometre scale. Nanostructured metallic multilayers enable precise tailoring of novel mechanical and functional coating properties by combining the desired characteristics of different individual materials. The resulting multilayers possess enhanced properties compared to the individual component materials. Crack growth, for instance, can be hindered by crack deflection along multilayer interfaces [16], resulting in increased fracture toughness. Further advantageous mechanical properties can be related to the confinement of nanograins in nano-scale strata, which hinder dislocation motion. Combining copper and tungsten in a nano-multilayer at a bilayer thickness ratio of 18:6 nm results in a coating material with high hardness, low thermal expansion coefficient and excellent thermal transport properties, which is of particular interest for thermal management applications at the micron scale. The immiscibility of Cu and W ensures clear phase separation along sharp interfaces. Further applications have been identified in the neutron radiation industry, where Cu/W multilayers could serve as shielding material [17]. For these applications, the mechanical integrity of the coating material is of utmost importance, as exposed substrate area might not provide sufficient shielding.

In this work, we present a novel approach for the determination of $K_{IC}$ in Cu/W nano-multilayers with a total thickness of 240 nm on Kapton substrate, which relies on surface displacement analysis obtained from Digital Image Correlations (DIC) analysis of SEM micrographs. We then confirm the validity of our approach with FEM modelling and benchmark the obtained $K_{IC}$ against the existing literature data.

## 2. Materials and Methods

### 2.1 Materials

Ten bilayers of Cu/W 18/6 nm were deposited onto 125 μm thick pre-cut Polyimide (Kapton) substrate in dog-bone shape (Figure 1b) for mechanical testing, resulting in a coating thickness of 240 nm. The deposition was carried out at room temperature by ion beam sputtering with a focused Ar + ion gun at 1.2 keV multicusp radio-frequency source in a NORDIKO-3000 system [18]. During film growth, the ion gun was supplied with constant radio-frequency power of 165 W and constant Ar flux of 10 standard cubic centimetre per minute (sccm). The 150 mm diameter targets were sputtered during 10 min allowing both ion-gun stabilization and target pollution cleaning caused by vacuum break. The ion gun axis was inclined at 45° to the normal of the surface target whilst the sample surface was parallel to the target plane. The sputtering chamber was pumped down to a base pressure of $2 \cdot 10^{-6}$ Pa whilst the working pressure during film growth was ~ $10^{-2}$ Pa. Substrates were preliminarily cleaned with acetone and ethanol and finally dried with an argon gas jet prior to their introduction in the deposition chamber. Tungsten and copper growth rates were previously calibrated by X-ray reflectometry (XRR) and were found to be 0.05 nm $s^{-1}$ and 0.16 nm $s^{-1}$, respectively. XRR was performed in order to evaluate sample stratification using the Bragg law at a grazing incidence angle. Energy-dispersive X-ray spectroscopy was used in a scanning electron microscope (SEM) to determine the atomic concentrations of Cu and W in the films and to estimate the effective tungsten and copper sublayer thicknesses per period employing the period obtained by XRR. The multilayer cross-section of a thin, electron-transparent lamella imaged using Scanning Transmission Electron Microscopy (STEM) at 20 keV beam energy shown in Figure 1a clearly reveals the multilayer structure with sharp Cu/W interfaces.

### 2.2 *In situ* uniaxial tensile experiment

The tensile specimen with dimensions shown in Figure 1b was clamped inside a uniaxial DEBEN *in situ* micro-tensile stage at a gauge length of 4 mm and mounted inside the chamber of a Tescan LYRA3 FIB-SEM instrument. To reduce aliasing and improve the DIC tracking, a grid of non-repetitive ‘sunflower’ pattern of dots shown in Figure 1c with a size of 11x11 $\mu m^2$ was deposited onto the surface of the sample using an in-chamber platinum deposition system [19]. As the pattern was formed of unconnected nano droplets, the fracture properties of the sample were not altered. To ensure crack growth across the patterned region of interest (ROI), an adjacent surface notch with the length of approximately 49 μm and width of approximately 0.3 μm was introduced using FIB at a beam current of 0.04 nA and at the accelerating voltage of 30 keV. The resulting surface preparation is shown in Figure 1d. A

small pre-existing flaw in form of a small crack in the ROI was identified and is marked with a yellow arrow.

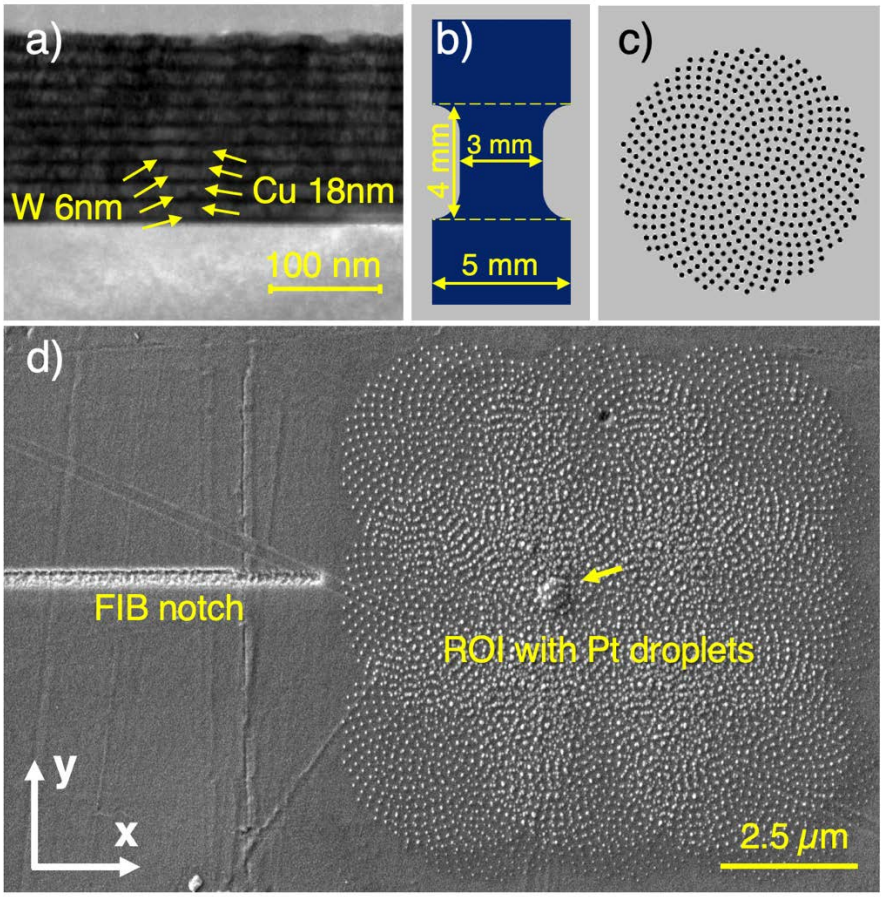


Figure 1 a) STEM Image of Cu/W multilayer cross-section showing clear layer separation between Cu (light) and W (dark). b) Dog bone specimen shape and dimensions. c) Non-repetitive sunflower pattern used to prevent DIC aliasing. d) Sample surface preparation for controlled crack growth and improved DIC tracking, including FIB notch (left) and Pt droplet pattern for improved DIC tracking (right). A small pre-existing crack in the coating is indicated with an arrow.

Subsequently, the sample was elongated by approximately 240 µm in 24 steps of 10 µm. Before the experiment and in between extension steps, high-resolution SEM images were acquired at the beam energy of 5 keV. Negligible sample relaxation in between loading steps was observed, as shown in the force versus displacement plot in Figure 2. The region of interest (ROI) with dimensions of 6x6 $\mu m^2$ on which the DIC markers were tracked is shown for four selected extension values corresponding to the labels in the left plot in Figure 2.

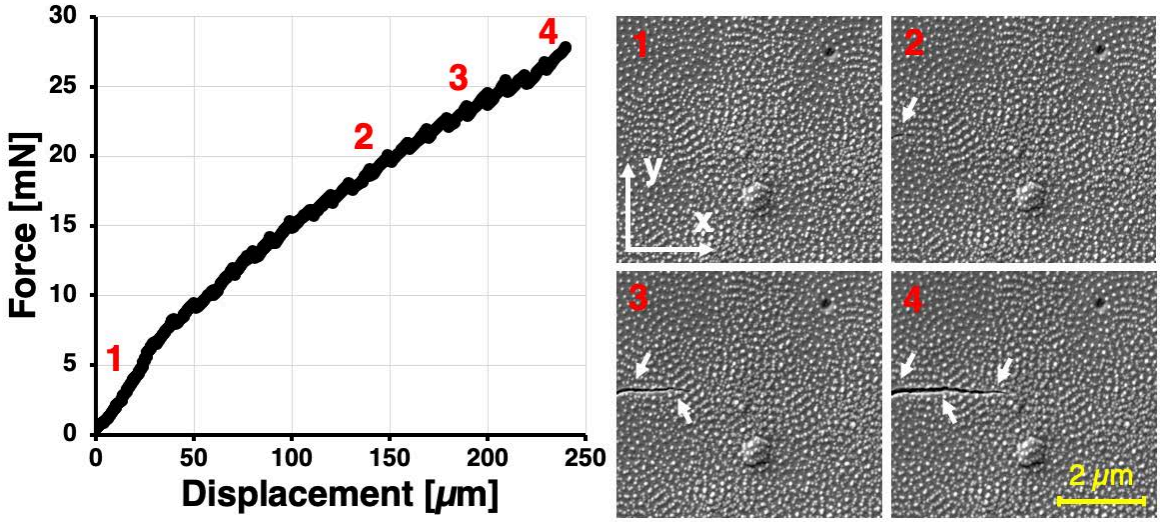


Figure 2. Left: Micro-tensile stage data showing elongation versus force during in situ tensile experiment. Right: DIC ROI at different elongations indicated in the force-displacement graph.

### 2.3 DIC analysis and fitting

To evaluate the displacement of surface markers with respect to the strain-free reference state, post-experimental DIC was carried out using a MATLAB-based software package [20]. The displacement field in x- and y-direction, $u_x$ and $u_y$, around the crack tip under plane stress assumption and Mode I loading can be expressed as [21]:

$$u_x = \frac{K_I}{2\mu}\sqrt{\frac{r}{2\pi}}\cos\left(\frac{\theta}{2}\right)\left[\frac{3-\nu}{1+\nu} - 1 + 2\sin^2\left(\frac{\theta}{2}\right)\right] \quad (1)$$

$$u_y = \frac{K_I}{2\mu}\sqrt{\frac{r}{2\pi}}\sin\left(\frac{\theta}{2}\right)\left[\frac{3-\nu}{1+\nu} + 1 - 2\cos^2\left(\frac{\theta}{2}\right)\right], \quad (2)$$

with the notations are $\mu$ for the shear modulus, and $\nu$ for Poisson's ratio.

The properties of Cu and W component materials are shown in Table 1, alongside the Cu/W mechanical properties obtained by the rule of mixture (Voigt model). The shear modulus of the

Cu/W 18/6 nm multilayer was calculated as $\mu_{Cu/W} = \frac{E_{Cu/W}}{2(1+\nu_{Cu/W})}$ according to the material constants provided in Table 1 [22], resulting in a value of $\mu_{Cu/W} = 59.6\ GPa$.

| | Young's Modulus E [GPa] | Poisson's Ratio $\nu$ |
|---|---|---|
| Cu (nano-crystalline) | 102 | 0.34 |
| W (nano-crystalline) | 338 | 0.36 |
| Cu/W 18/6 | 161 | 0.35 |

Table 1. Material properties used for $K_{IC}$ fitting

**2.4 Numerical Simulation**

A fundamental hypothesis made in the experimental determination of the critical stress intensity factor via DIC was that $K'$ evaluated from the surface displacement of the coating around the crack tip during propagation is representative of $K''$ in the coating in the absence of the substrate, i.e. $K' = K''$. This hypothesis was thoroughly tested and validated in the present study through modelling and comparison with literature data, so that the validity of the obtained $K_{IC}$ from DIC for the isolated coating was verified. Two independent FEM simulations under plane stress assumption were created using COMSOL Multiphysics package. In order to evaluate whether full-field fitting of the coating displacement and stress fields ahead of the crack tip lead to identical results independent of the substrate, Model 1 was simulated as a thin film on compliant substrate, while Model 2 was simulated as free-standing coating, as shown in Figure 3. In a first step, a fixed displacement was applied to Model 1, resulting in a stress intensity $K_I$ at the crack tip. Subsequently, a fixed displacement for Model 2 was found iteratively, resulting in a matching $K_I$ value. Finally, the two displacement fields were compared in order to verify whether these also deliver the identical $K_I$ based on LEFM fitting.

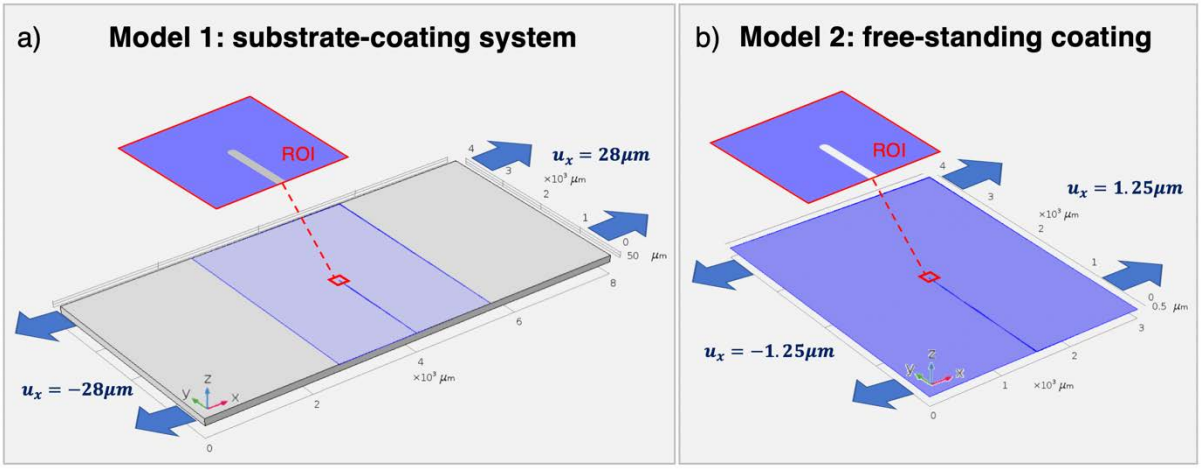


Figure 3a. COMSOL Model 1 geometry overview showing Kapton substrate (grey) with Cu/W coating (blue). Blue arrows indicate prescribed uniaxial displacement. ROI highlighted in red. b. COMSOL Model 2 geometry overview showing free standing Cu/W coating (blue).

For Model 1, a Kapton substrate with dimensions of 8000x4000x125 $\mu m^3$ was generated and coated with a thin film of dimensions 3000x4000x1 $\mu m^3$. Perfect adhesion at the substrate-coating interface was assumed, since no coating debonding was observed during the *in situ* experiment. An elongated notch was introduced into the coating with a crack tip radius of 1 µm and a length of 2000 µm, as shown in Figure 3a. A prescribed symmetric total displacement of 56 µm in x-direction at the substrate ends was applied, resulting in an overall substrate strain of around 0.7%. In addition, rigid motion suppression for the entire model was applied in order to prevent translational and rotational motions. While the material parameters shown in Table 1 were used for the coating, a strain-dependent Young's modulus was implemented to model a realistic elasto-plastic behaviour of the Kapton substrate. Based on the force-strain data shown in Figure 2 and a known sample cross-sectional area of 3000x125 $\mu m^2$, the Young's modulus in the linear-elastic region up to $\varepsilon = 0.9\%$ was determined as $E_1$ = 2 GPa, while it was found to be $E_2$ = 0.94 GPa in the region beyond $\varepsilon = 0.9\%$. A Poisson's ratio of $\nu = 0.35$ was used based on Kapton manufacturer data [23]. Identical coating material parameters were used for Model 2, which simulated a piece of free stranding coating of the same dimensions as described in Model 1 as is shown in Figure 3b. The ROI around the crack tip is highlighted in red. A prescribed symmetric total displacement of 2.5 µm in x-direction was applied at the sample ends in order to match the stress intensity at the crack tip obtained from Model 1.

## 3. Results and Discussion

### 3.1 DIC fitting

The displacement fields $u_x$ and $u_y$ obtained from DIC analysis of experimental data at loading step 4 in Figure 2 are shown in Figure 4a and Figure 4c. Nonlinear least square fitting was used to determine the critical stress intensity factor describing the displacement field around the Mode I crack opening according to equations (1) and (2), which returned a value of $K_{IC} = 4.8 \pm 0.05\ \mathrm{MPa}\sqrt{\mathrm{m}}$ for $u_x$ and $K_{IC} = 4.8 \pm 0.02\ \mathrm{MPa}\sqrt{\mathrm{m}}$ for $u_y$ in a 95% confidence interval. The resulting displacement field fits based on linear-elastic fracture mechanics for $u_x$ and $u_y$ are shown in Figure 4b, d.

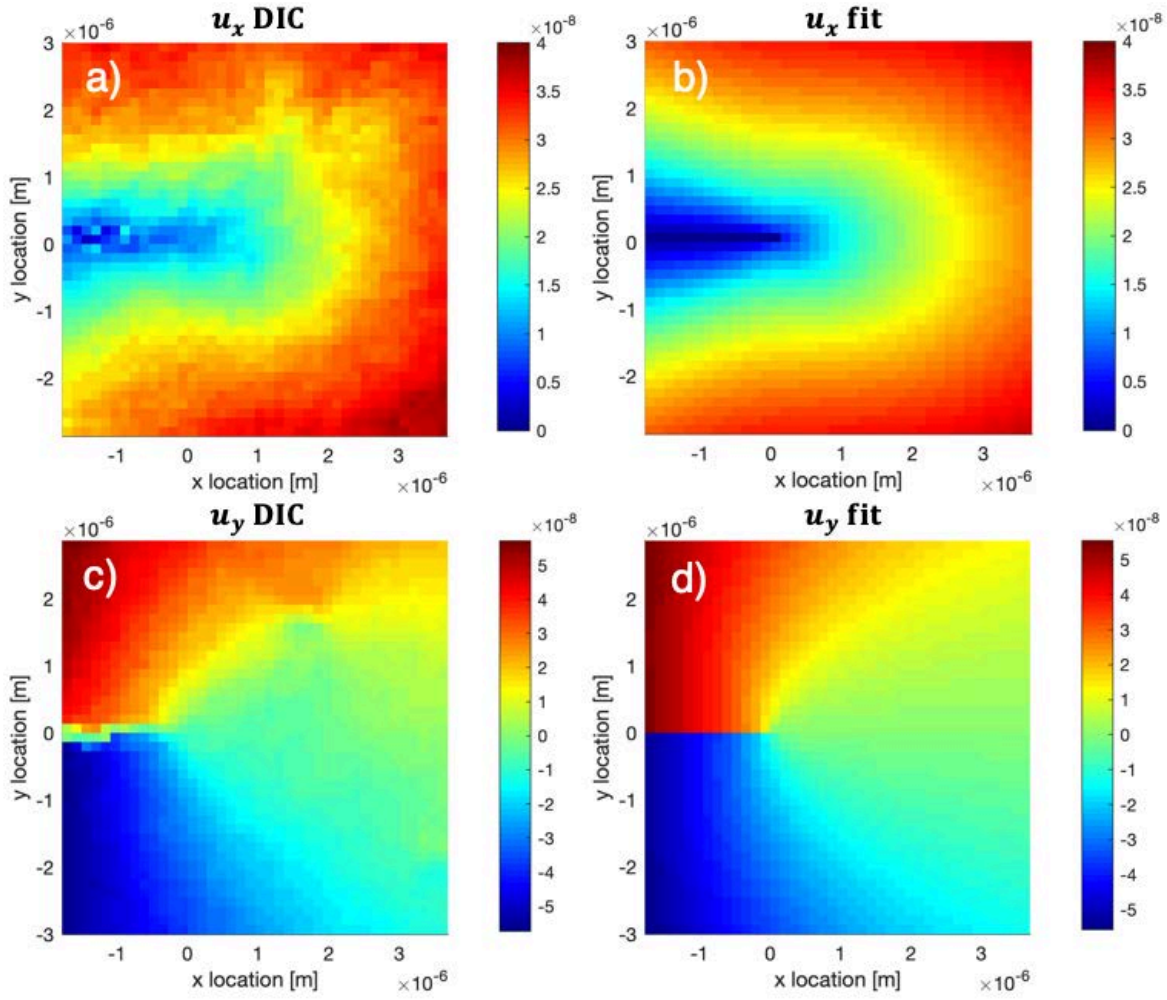


Figure 4. Results of DIC analysis alongside fitted results predicted by LEFM. a) DIC results of displacement in x direction b) Fit of x-displacement field based on linear elastic fracture mechanics for $K_{IC} = 4.8 \pm 0.05\ \mathrm{MPa}\sqrt{\mathrm{m}}$. c) DIC results of displacement in y direction. d)

Fit of y-displacement field based on linear elastic fracture mechanics for $K_{IC} = 4.8 \pm 0.02$ MPa$\sqrt{\text{m}}$.

To verify the obtained $K_{IC}$ value, the result was compared to literature data obtained using different testing methods on similar systems. While no values for the fracture toughness of Cu/W nano-multilayers could be found in the literature, extensive data for pure Cu thin films of different thicknesses was published by Hirakata et al. [24] and Keller et al. [25]. The result comparison shown in Figure 5 confirms a fracture toughness property of Cu/W nano-multilayers very close to the expected $K_{IC}$ for a pure Cu film of identical thickness. As the Cu/W 18/6nm nano-multilayer consists of 75% Cu by thickness, a material behaviour close to Cu appears reasonable. A square root dependence between film thickness t and the critical stress intensity was found, which can be described as [11]

$$K_{I,C} = \sqrt{0.5 E k_{sl} t}, \tag{3}$$

with $k_{sl}$ as single fit parameter representing the effective stress resistance to shear lip formation. The corresponding fit shown as dotted line in Figure 5 returned a value of $k_{sl} = 1.19 \pm 0.03 \frac{GJ}{m^3}$ for Cu/W 18/6, which can also be thought of shear fracture stress of $1.19 \pm 0.03\ GPa$. Furthermore, the size-dependent fracture properties of pure W micro-cantilevers studied by Ast et al. [26] indicate a similar fracture toughness range between 3 MPa$\sqrt{\text{m}}$ for single crystalline W up to around 6 MPa$\sqrt{\text{m}}$ for nanogranular W with a grain size of around 790 nm. Finally, further studies on the fracture toughness of Cu/Cr nano-multilayers with different bilayer periods [27] showed a very close critical stress intensity factor of around 5 MPa$\sqrt{\text{m}}$ for a Cu/Cr nano-multilayer with an individual layer thickness of 12.5 nm.

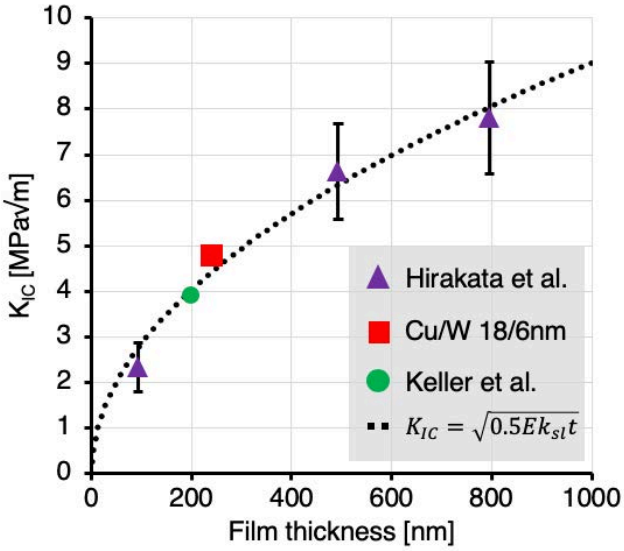


Figure 5. Comparison of the obtained $K_{IC}$ for Cu/W with literature data on free-standing Cu thin films vs. film thickness. Dotted line: square root fit of the literature data according to equation (3).

3.2 Simulation results

The resulting horizontal stress component distributions $\sigma_{xx}$ for both Model 1 and Model 2 are shown in Figure 6. While a stress concentration at the notch tip can be observed in both models, the horizontal stress $\sigma_{xx}$ in Model 2 is overall significantly lower as compared to Model 1. The driving force underlying the elevated overall stress level in Model 1 is the adhesion between substrate and coating, which leads to stress transfer across the interface through shear deformation of the substrate. A detailed description of this mechanism based on the shear lag theory can be found in [18,28]. The following analysis will be focused on the question whether the stress and displacement fields in the ROI labelled '2' in Figure 6 are comparable for both Model 1 and Model 2.

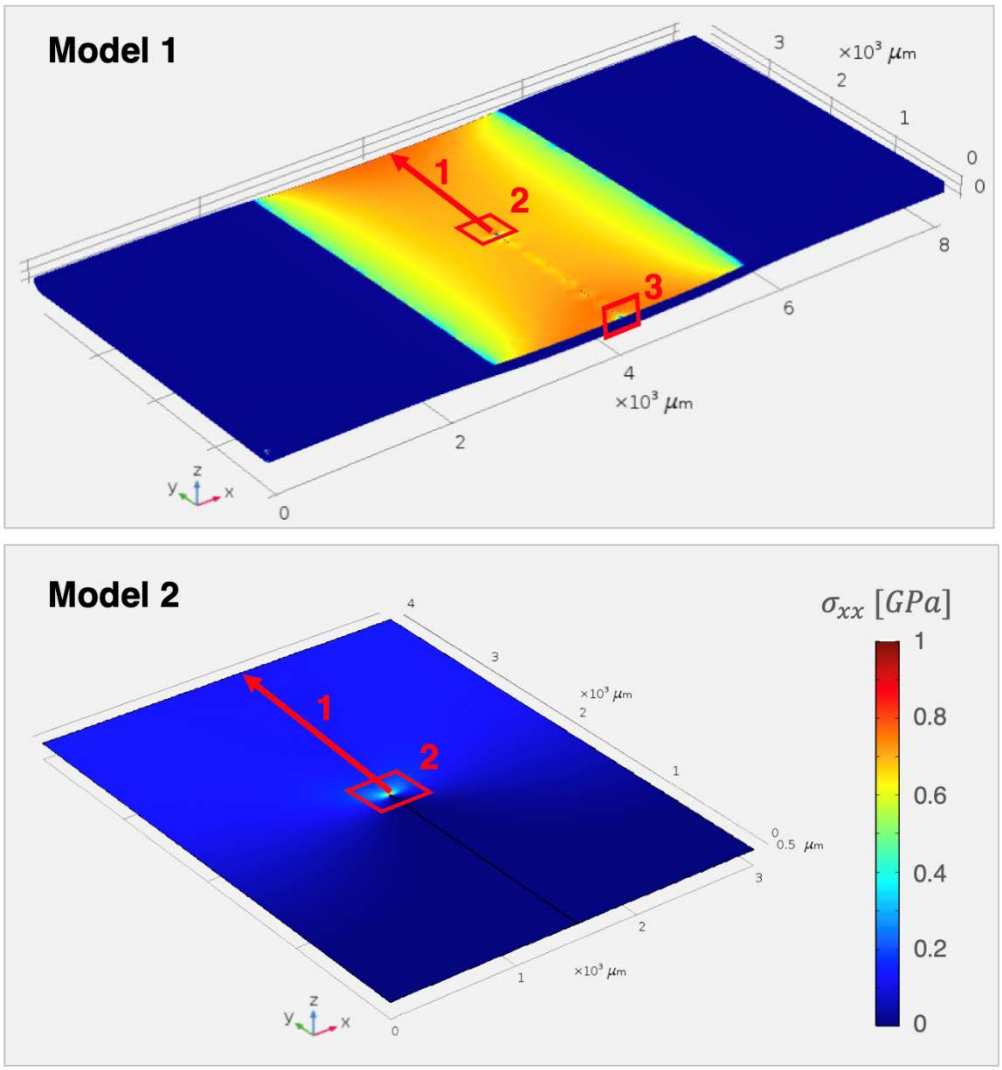


Figure 6. Resulting horizontal stress $\sigma_{xx}$ from prescribed displacement at the sample end for Model 1 (substrate-coating system) and model 2 (free-standing coating). 1: location and direction of $\sigma_{xx}$ line plot. 2: Region of interest for full field fitting. 3: Region of interest for the analysis of substrate stress.

In a first step, the singularity dominated region or K-field was identified, in order to fit the stress intensity factor $K_I$. For this purpose, the line profiles of the horizontal stress distribution $\sigma_{xx}$ ahead of the notch tip were compared for both Model 1 and Model 2 along the direction labelled '1' in Figure 6. The result shown as double-logarithmic plot in Figure 7 shows identical stress behaviours for both models in the region ranging from the notch tip up to a distance of around 5.5 µm. Both curves can be subdivided into three distinct regions [29]: the plastic zone in close proximity of the notch tip labelled 'A', the linear region representing the K-field labelled 'B', and the far field dominated by the sample constraints labelled 'C' for the substrate-

coating system. It is clearly visible that the linear region suitable for the determination of the stress intensity factor is significantly larger in Model 2, while the stress distribution in Model 1 beyond 5.5 µm from the notch tip is dominated by the stress transferred from the substrate to the coating. Based on this information, a region of interest ranging from 0.25 µm to 5.5 µm ahead of the crack tip was selected for further analysis and full-field fitting of the displacement and stress fields.

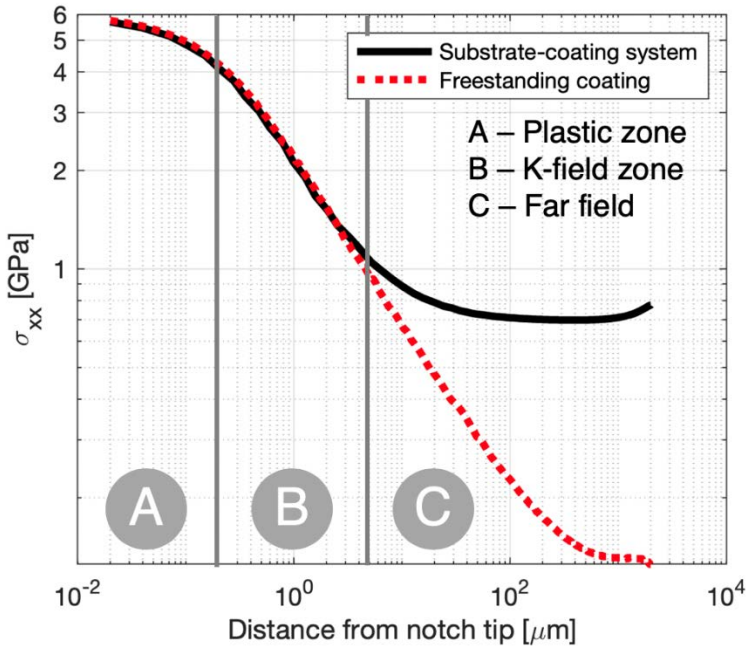


Figure 7. Double-logarithmic line profile of the horizontal stress component $\sigma_{xx}$ in y-direction ahead of the notch tip. Stress values for the substrate-coating system (Model 1) are displayed as solid black line, stress values for the free-standing coating (Model 2) are displayed as dotted red line. A subdivision of different zones for the substrate-coating system (Model 1) are labelled as A, B and C, representing the plastic zone, K-field and far field.

Subsequently, the stress field $\sigma_{xx}$ in the region labelled 'B' in Figure 7 was fitted for both models using the following relation based on linear-elastic fracture mechanics [21]:

$$\sigma_{xx} = \frac{K_I}{\sqrt{2\pi r}} \cos\left(\frac{\theta}{2}\right)\left[1 + \sin\left(\frac{\theta}{2}\right)\sin\left(\frac{3\theta}{2}\right)\right] \tag{4}$$

The fits shown as surface plot in Figure 8 reveal identical stress and displacement behaviours for both Model 1 and Model 2 in the singularity dominated zone. Non-linear least square fitting

of the simulation results revealed the stress intensity values based on the stress field $\sigma_{xx}(x, y)$ and the displacement field $u_x(x, y)$. Identical stress intensity values of $K_I = 5.027 \pm 0.063\ MPa\sqrt{m}$ were obtained for all four sets of simulation data.

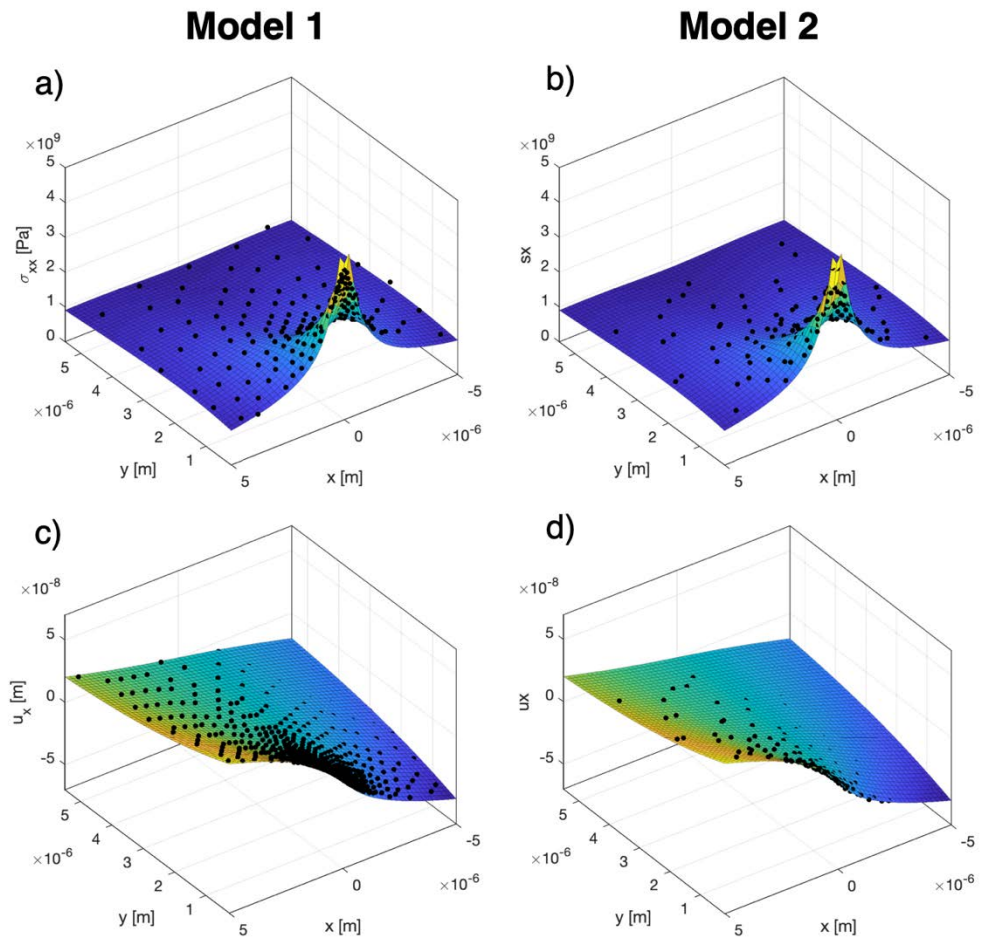


Figure 8. Simulation results (black markers) and fits (surface plots) of stress and displacement fields in the singularity dominated zone for Model 1 and Model 2. a) Stress field ahead of the crack tip for Model 1. b) Stress field ahead of the crack tip for Model 2. c) Displacement field ahead of the crack tip for Model 1. d) Displacement field ahead of the crack tip for Model 2.

The above-presented results clearly indicate that estimating the stress intensity factor of coating material is possible based on the surface displacement field of a coating-substrate system in which only the substrate experiences external loading. However, this approach is only valid in the K-field dominated zone ahead of the crack tip, which can be identified as a linear region in a double-logarithmic plot of the stress field ahead of the crack tip, as shown in Figure 7. The large difference in stress in the far field region ('C' in Figure 7) clearly shows the limits of this

technique, as only a small region close to the notch tip can be used for the analysis carried out above. High-resolution microscopic imaging techniques as used in this study are therefore required to capture the displacement at the scale of the K-field size.

Finally, the behaviour of the coating-substrate interface (region '3' in Figure 6) was studied based on simulation results. A high concentration of stress $\sigma_{xx}$ in horizontal direction around the notch opening was found, as shown in Figure 9. The coating gap was found to act as 'crack tip' reaching vertically into the substrate. The stress levels found in the substrate near the crack opening exceed the linear elastic regime of the substrate by far and lead to local plastic deformation. As the substrate becomes significantly more compliant when stretched beyond its yield point, the stress concentration along the substrate-coating interface permits further crack opening resulting in a higher stress concentration at the notch tip, despite the strong substrate-coating bond. The displacement field near the crack tip and crack opening is therefore mainly representative of the coating material, as the plastically deformed substrate does not restrain the coating in this zone. At further distance from the crack, the substrate-coating bond is intact and continues to drive the crack growth and opening. It is thus possible to use the near-crack region for $K_{IC}$ determination of the coating material.

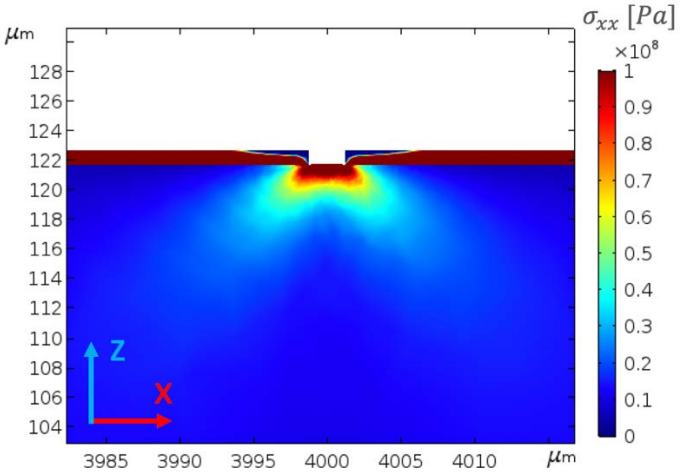


Figure 9. Horizontal stress distribution at the substrate coating interface around the notch opening revealing high level of stress concentration in the substrate.

## 4. Conclusion

A multi-step approach for the determination of the Mode I critical stress intensity factor $K_{IC}$ in Cu/W nano-multilayers on compliant Kapton substrate based on DIC analysis of controlled

uniaxial crack growth was presented in this work. 2D displacement field fitting in close proximity of the crack tip based on linear elastic fracture mechanics was used to obtain the critical stress intensity factor of $K_{\mathrm{IC}} = 4.8 \pm 0.05\ \mathrm{MPa}\sqrt{\mathrm{m}}$. Excellent agreement with literature values for pure Cu thin films of similar thickness as well as Cu/Cr nano-multilayers of similar bilayer period was found.

To confirm the validity of the chosen approach, two independent FEM simulations were developed and compared. The first model simulated a thin film on compliant substrate. The second model simulated a free standing thin film of the same dimensions. By applying a prescribed displacement at both ends of the first model, thus imitating the experimental setup with a micro-tensile stage, a stress intensity at the crack tip was created. A matching stress intensity was then iteratively found for model 2 by applying a fixed displacement. In order to identify whether the displacement field ahead of the crack tip in the substrate-coating model is representative of the mechanical properties of the coating material, both the displacement and stress field were compared across both simulations. Identical stress intensity factors were found across both simulations for a limited region dominated by the K-field. The experimental determination via DIC was therefore confirmed as appropriate. Finally, the mechanisms permitting crack opening despite a strong substrate-coating bond were revealed based on the simulation of the substrate-coating system, according to which local plastic deformation of the substrate is permitting the crack to open and grow.

**Acknowledgements**

AMK wishes to acknowledge the support for this research through EPSRC project EP/S005072/1 “ASiMoV”.

**Conflicts of interest**

There are no conflicts of interest to declare.

## References


[1] G. Abadias, E. Chason, J. Keckes, M. Sebastiani, G.B. Thompson, E. Barthel, G.L. Doll, C.E. Murray, C.H. Stoessel, L. Martinu, Review Article: Stress in thin films and coatings: Current status, challenges, and prospects, J. Vac. Sci. Technol. A Vacuum, Surfaces, Film. 36 (2018) 020801. doi:10.1116/1.5011790.

[2] S. Zhang, X. Zhang, Toughness evaluation of hard coatings and thin films, Thin Solid Films. 520 (2012) 2375–2389. doi:10.1016/j.tsf.2011.09.036.

[3] E. Hintsala, & D. Kiener, & J. Jackson, W.W. Gerberich, In-Situ Measurements of Free-Standing, Ultra-Thin Film Cracking in Bending, (n.d.). doi:10.1007/s11340-015-0069-2.

[4] G. Jaeger, I. Endler, M. Heilmaier, K. Bartsch, A. Leonhardt, New method of determining strength and fracture toughness of thin hard coatings, Thin Solid Films. 377–378 (2000) 382–388. doi:10.1016/S0040-6090(00)01312-2.

[5] Z. Chen, Z. Gan, Fracture toughness measurement of thin films on compliant substrate using controlled buckling test, Thin Solid Films. 515 (2007) 3305–3309. doi:10.1016/j.tsf.2006.01.044.

[6] Z. Chen, B. Cotterell, W. Wang, The fracture of brittle thin films on compliant substrates in flexible displays, Eng. Fract. Mech. 69 (2002) 597–603. doi:10.1016/S0013-7944(01)00104-7.

[7] A. Favache, C.H. Sacré, M. Coulombier, L. Libralesso, P. Guaino, J.P. Raskin, C. Bailly, B. Nysten, T. Pardoen, Fracture mechanics based analysis of the scratch resistance of thin brittle coatings on a soft interlayer, Wear. 330–331 (2015) 461–468. doi:10.1016/j.wear.2015.01.081.

[8] A.A. Voevodin, J.S. Zabinski, Supertough wear-resistant coatings with “chameleon” surface adaptation, Thin Solid Films. 370 (2000) 223–231. doi:10.1016/S0040-6090(00)00917-2.

[9] C.L. Li, J.P. Chu, J.W. Lee, Measuring notch toughness of thin film metallic glasses using focused ion beam-based microcantilever method: Comparison with Ti and TiN crystalline films, Mater. Sci. Eng. A. 698 (2017) 104–109. doi:10.1016/j.msea.2017.05.002.

[10] J. Ast, T. Przybilla, V. Maier, K. Durst, M. Göken, Microcantilever bending experiments in NiAl - Evaluation, size effects, and crack tip plasticity, J. Mater. Res. 29 (2014) 2129–2140. doi:10.1557/jmr.2014.240.

[11] E.I. Preiß, B. Merle, M. Göken, Understanding the extremely low fracture toughness of freestanding gold thin films by in-situ bulge testing in an AFM, Mater. Sci. Eng. A. 691 (2017) 218–225. doi:10.1016/j.msea.2017.03.037.

[12] T.Y. Tsui, Y.C. Joo, A new technique to measure through film thickness fracture toughness, Thin Solid Films. 401 (2001) 203–210. doi:10.1016/S0040-6090(01)01613-3.

[13] P. Jedrzejowski, J.E. Klemberg-Sapieha, L. Martinu, Relationship between the mechanical properties and the microstructure of nanocomposite TiN/SiN1.3 coatings prepared by low temperature plasma enhanced chemical vapor deposition, Thin Solid Films. 426 (2003) 150–159. doi:10.1016/S0040-6090(03)00028-2.

[14] E. Salvati, T. Sui, A.J.G. Lunt, A.M. Korsunsky, The effect of eigenstrain induced by ion beam damage on the apparent strain relief in FIB-DIC residual stress evaluation, Mater. Des. 92 (2016) 649–658. doi:10.1016/j.matdes.2015.12.015.

[15] E. Salvati, L.R. Brandt, C. Papadaki, H. Zhang, S.M. Mousavi, D. Wermeille, A.M. Korsunsky, Nanoscale structural damage due to focused ion beam milling of silicon with Ga ions, Mater. Lett. 213 (2018). doi:10.1016/j.matlet.2017.11.043.

[16] R. Bermejo, R. Danzer, High failure resistance layered ceramics using crack bifurcation and interface delamination as reinforcement mechanisms, Eng. Fract. Mech. 77 (2010) 2126–2135. doi:10.1016/j.engfracmech.2010.02.020.

[17] Y. Gao, T. Yang, J. Xue, S. Yan, S. Zhou, Y. Wang, D.T.K. Kwok, P.K. Chu, Y. Zhang, Radiation tolerance of Cu/W multilayered nanocomposites, J. Nucl. Mater. 413 (2011) 11–15. doi:10.1016/j.jnucmat.2011.03.030.

[18] L.R. Brandt, E. Salvati, C. Papadaki, H. Zhang, S. Ying, E. Le Bourhis, I. Dolbnya, T. Sui, A.M. Korsunsky, Probing the deformation and fracture properties of Cu/W nano-multilayers by in situ SEM and synchrotron XRD strain microscopy, Surf. Coat. Technol. 320 (2017) 158–167. doi:10.1016/j.surfcoat.2017.01.065.

[19] H. Vogel, A better way to construct the sunflower head, Math. Biosci. 44 (1979) 179–189. doi:10.1016/0025-5564(79)90080-4.

[20] C. Eberl, Digital Image Correlation and Tracking, MATLAB Cent. File Exch. (2020). https://www.mathworks.com/matlabcentral/fileexchange/12413-digital-image-correlation-and-tracking (accessed July 22, 2020).

[21] T.L. Anderson, Fracture Mechanics: Fundamentals and Applications, Fourth Edition, Fourth, CRC Press, 2017.

[22] L. Romano-Brandt, E. Salvati, E. Le Bourhis, T. Moxham, I.P. Dolbnya, A.M.

Korsunsky, Nano-scale residual stress depth profiling in Cu/W nano-multilayers as a function of magnetron sputtering pressure, Surf. Coatings Technol. 381 (2020) 125142. doi:10.1016/j.surfcoat.2019.125142.

[23] DuPont, DuPont Kapton HN, (2019) 2. https://www.dupont.com/content/dam/dupont/amer/us/en/products/ei-transformation/documents/DEC-Kapton-HN-datasheet.pdf (accessed July 27, 2020).

[24] H. Hirakata, O. Nishijima, N. Fukuhara, T. Kondo, A. Yonezu, K. Minoshima, Size effect on fracture toughness of freestanding copper nano-films, Mater. Sci. Eng. A. 528 (2011) 8120–8127. doi:10.1016/j.msea.2011.07.071.

[25] R.R. Keller, J.M. Phelps, D.T. Read, Tensile and fracture behavior of free-standing copper films, Mater. Sci. Eng. A. 214 (1996) 42–52. doi:10.1016/0921-5093(96)10253-7.

[26] J. Ast, M. Göken, K. Durst, Size-dependent fracture toughness of tungsten, Acta Mater. 138 (2017) 198–211. doi:10.1016/j.actamat.2017.07.030.

[27] J.Y. Zhang, G. Liu, X. Zhang, G.J. Zhang, J. Sun, E. Ma, A maximum in ductility and fracture toughness in nanostructured Cu/Cr multilayer films, Scr. Mater. 62 (2010) 333–336. doi:10.1016/j.scriptamat.2009.10.030.

[28] Y. Liu, I. Bhamji, P.J. Withers, D.E. Wolfe, A.T. Motta, M. Preuss, Evaluation of the interfacial shear strength and residual stress of TiAlN coating on ZIRLO™ fuel cladding using a modified shear-lag model approach, J. Nucl. Mater. 466 (2015) 718–727. doi:10.1016/j.jnucmat.2015.06.003.

[29] L. Vergani, Meccanica dei materiali, McGraw-Hill Companies, 2006.

## Author Biographies

León Romano Brandt

León Romano Brandt is a DPhil (Doctor of Philosophy) student in Engineering Science at St Hugh's College Oxford. He obtained his Bachelor of Science in Engineering Science from Technical University Munich in 2015, before joining the Korsunsky Group at the University of Oxford. His research interest lies in the mechanical and thermal properties of nano-crystalline thin film and energy materials at the micro- and nano scale using synchrotron and FIB-SEM/TEM techniques. To date, he has authored and co-authored 14 journal articles.

Enrico Salvati

Enrico Salvati is an Assistant Professor (Tenure-Track) at the Polytechnic Department of Engineering and Architecture (DPIA) of the University of Udine. He completed his doctorate (DPhil) at the Engineering Science department of the University of Oxford (2017). His research group focuses mainly on the development of design against failure criteria and damage tolerant design approaches, particularly for processed, welded and additively

manufactured materials. This research is carried out using FEM modelling coupled with a wide range of experimental techniques able to probe materials at different length scales.

Eric Le Bourhis

Eric Le Bourhis is professor at Poitiers University (France). He gained his PhD at Paris VII University in 1994, then joined Saint Gobain R&D as an engineer when he applied contact mechanics to glass surfaces and coatings developed for glazing. He joined Poitiers University in 1998, where he has pursued an activity to promote sol-gel hybrid coatings in close collaboration with glass industrial manufacturers, while his other research activities focus on the mechanical properties of thin-films and nanostructures. He has published 200 papers in international journals, 4 patents and 1 book (Glass Mechanics and Technology, Wiley VCH, 2014).

Alexander Korsunsky

Professor Alexander Korsunsky is a world-leader in engineering microscopy of materials for optimisation of design, durability and performance. He leads the MBLEM lab (Multi-Beam Laboratory for Engineering Microscopy) at Oxford, and the Centre for In situ Processing Science (CIPS) at the Research Complex, Harwell. He consults Rolls-Royce plc on matters of residual stress and structural integrity, and is Editor-in-Chief of Materials & Design, a major Elsevier journal (2019 impact factor 6.289). Alexander holds the degree of Doctor of Philosophy (DPhil) from Merton College, Oxford. He was Junior Research Fellow at Fitzwilliam College, Cambridge, and Lecturer at Newcastle University, before returning to Oxford.